LBL-10110 c2

Lawrence Berkeley Laboratory
UNIVERSITY OF CALIFORNIA

Materials & Molecular Research Division

Presented at the 1978 TMS-AIME Fall Meeting, St. Louis, MO, October 15-19, 1978

THE EFFECTS OF THE MICROSTRUCTURE OF DUCTILE ALLOYS ON SOLID PARTICLE EROSION BEHAVIOR

Alan V. Levy and Said Jahanmir

October 1978

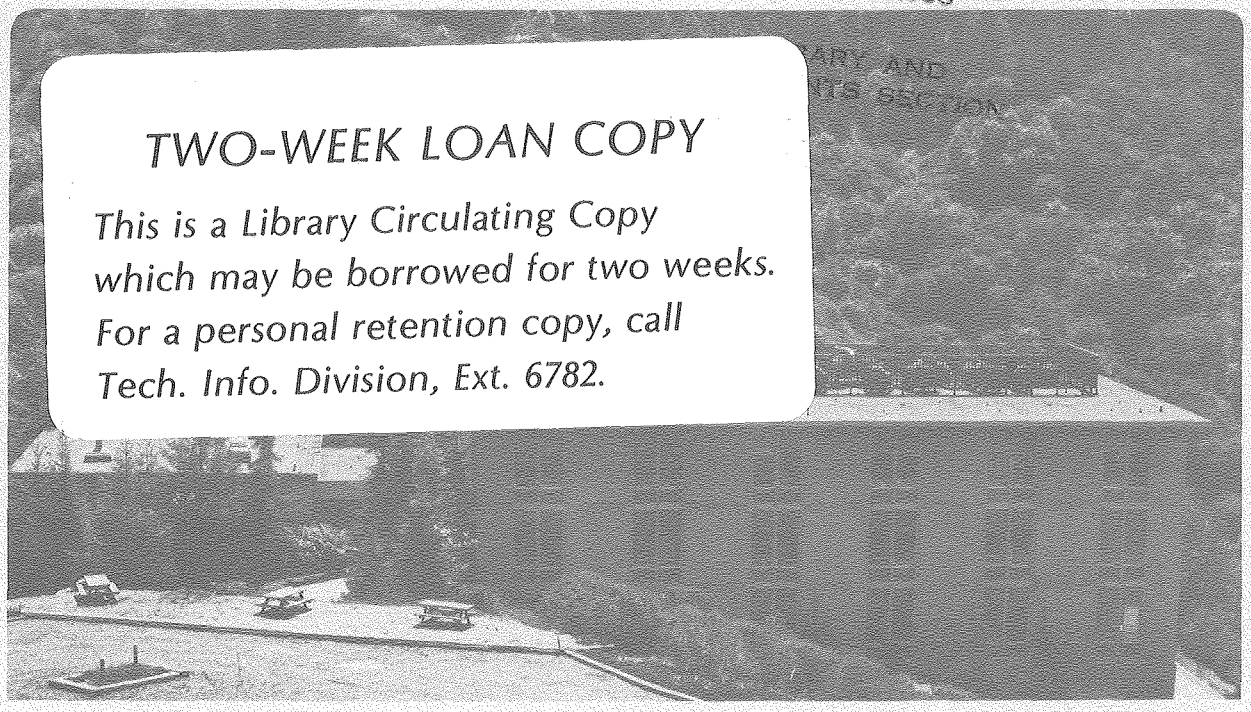

Prepared for the U.S. Department of Energy under Contract W-7405-ENG-48

DISCLAIMER

THE EFFECTS OF THE MICROSTRUCTURE OF DUCTILE ALLOYS ON SOLID PARTICLE EROSION BEHAVIOR*

Alan V. Levy
Lawrence Berkeley Laboratory
Berkeley, CA 94720

and

Said Jahanmir
Cornell University
Ithaca, N. Y.

Abstract

The effect of microstructure of two phase alloys, consisting of a softer, ductile matrix and a harder interspersed phase, on erosion behavior was determined. The stress and strain distribution in a two phase alloy where the second, hard phase is a distribution of particles in a more ductile matrix was calculated. It was determined that a spheroidized 1075 carbon steel eroded 30 percent less than a pearlitic microstructure of the same steel even though the spherodized form was 21 R_B points of hardness lower than that of the pearlitic steel. The computerized calculation of stresses and strains from the impact of eroding particles on a two phase alloy surface were used to define the ability of the particle impact to induce voids and cracks in the target material that could cause material loss. The resultant predicted voids and cracks were related to experimentally determined behavior of spherodized steel.

* This work was supported by the Materials Science Division, Office of Basic Energy Sciences, Department of Energy under Contract No. W-7405-ENG-48.

Introduction

The study of gas-solid particle erosion of metals has primarily concentrated on measuring the loss rate of different metals subjected to varying erosion conditions and defining the loss in analytical expressions that address the mechanical nature of the process (1-6). Relatively little work has been done to investigate the effect of the microstructure of metals on erosion behavior.

It is the purpose of this investigation to vary the microstructure of the target material to determine its effect on solid particle erosion and to examine microscopically subsurface deformation caused by the erosion process using SEM. The approach taken was to select an alloy that could be readily heat treated to different microstructures without changing drastically the hardness of the material. The alloy chosen for the erosion study was a commercial plain carbon 1075 steel (7). The steel was chosen because it could be heat treated to a lamellar structure and a spheroidized structure making it possible to examine the effect of fine pearlite, coarse pearlite, and the spheroidized structure on erosion.

Specimen Preparation

A commercial plain carbon 1075 steel was obtained for erosion testing and cut into samples 0.75 in. x 2.5 in. x 0.125 in. The steel was heat treated to fine pearlite, coarse pearlite, and spheroidized microstructures (Figure 1) in a high vacuum controlled atmosphere furnace to prevent chemical changes on the sample surface. The three microstructures were formed by austenitizing the steel at 875° ± 3°C for 30 minutes and

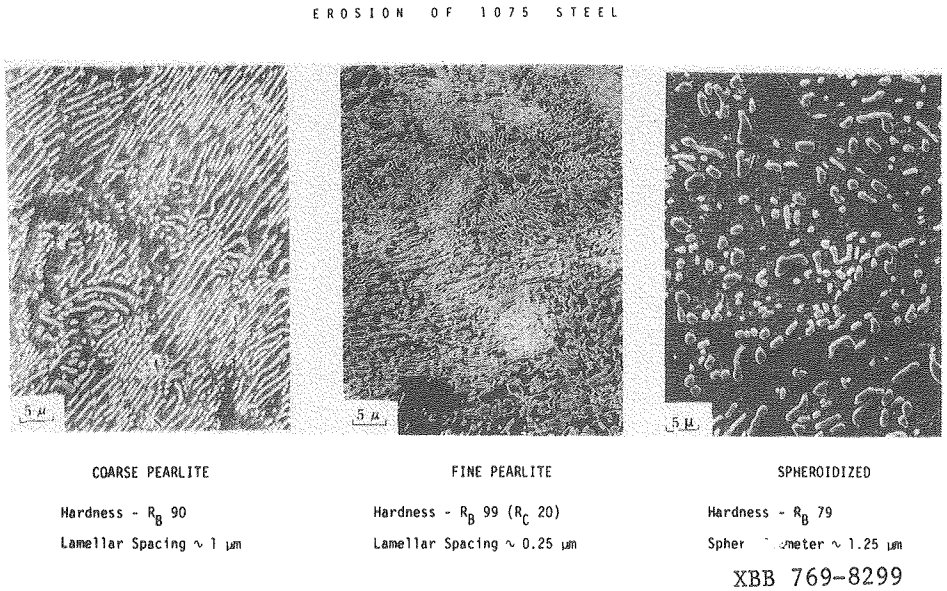

Fig. 1 - Scanning electron micrographs of 1075 steel in the coarse pearlite, fine pearlite and spheroidized microstructures

subsequently cooling at a rate that would develop the desired microstructure.

Samples used for multiple particle impact testing were metallographically polished through a 4/0 paper prior to testing. Those used for single particle impact studies were polished through 1 μm diamond wheel.

Erosion Testing

The erosion testing was conducted at room temperature using an air blast tester shown in Figure 2. The tester operated by feeding the eroding particles from a vibrating hopper into a stream of gas. The particle feed rate was found to be accurate and constant at 20 grams/minute, a solid loading of 0.06 gm SiC/gm air at 30.5 mps (100 fps) and 0.36 gm SiC/gm air at 61 mps (200 fps) for the size and shape of particles used in this study. Angular silicon carbide particles were used as the eroding material having a hardness of about 4500 (VHN) and an actual (true) density of 3.2 grams/cm^3. Most erosion testing was conducted using +65 -60 mesh (240 μm diameter) particles. The testing device allowed for choice of particle velocity by changing the pressure drop and gas flow rate across a 0.305 m (12") long by 4.77 mm (0.1875") ID stainless steel nozzle. Particle velocities used in this study were 30.5 mps (100 fps) and 61 mps (200 fps). These velocities were calculated using a one dimensional, two phase flow computer analysis (8) and experimentally verified using a rotary disc testing device (9). Angles of impingement used in this study were 15°, 30°, and 90°.

Single particle and multiple particle erosion tests were conducted on the steel samples. Single particle impact craters were observed with the SEM and stereo photomicrographs were taken to determine the depth of the craters. The multiple particle impact tests were conducted by impacting five, 60 gram charges of SiC on the sample surface with weight loss measurements of the sample taken after each 60 gram charge. After each 60 grams impacted, the surface was subjected to a high pressure air blast to minimize the amount of SiC left on the surface before weight measurements were taken. A total of 300 grams (five charges) of SiC was used in eroding each sample. Erosion rates for each successive 60 gram charge of SiC were determined by the formula:

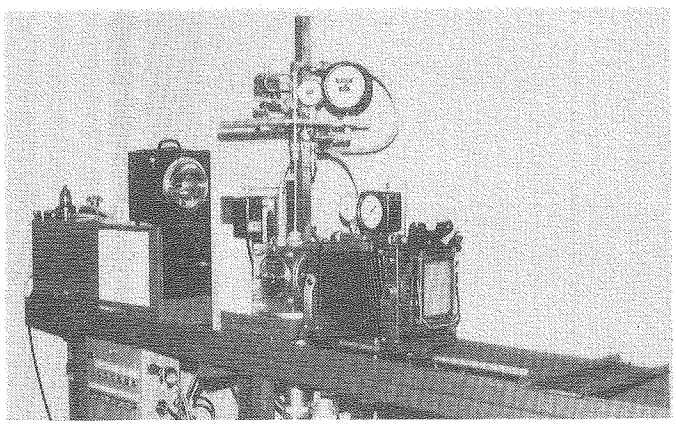

CBB 763-2073

Fig. 2 -Photograph of room temperature erosion tester.

$$\text{Erosion Rate} = \frac{\text{change in mass of sample}}{\text{mass of impacting particles (60 gm)}}$$

Test Results/Discussion

Erosion Tests

Results of a typical multiple particle erosion test for the three different microstructures of the 1075 steel are shown in Figure 3. This curve was made for a test particle velocity of 30.5 mps (100 fps) and an angle of impingement of 30°. The curve shows that after steady state erosion had begun (the horizontal portion of the curve) the spheroidized microstructure eroded less than either the coarse or fine pearlite. It should also be noted that there is a definite threshold region of increasing erosion rate before steady state erosion begins. Erosion data at a particle velocity of 61 mps (200 fps) also show that the spheroidized structure eroded less than the fine or coarse pearlite structures.

Erosion rates can be compared for the three microstructures at all angles of impingement on an erosion rate vs angle of impingement curve for 30.5 mps, (Figure 4). The curves are typically shaped for ductile alloys. Data scatter bands for 15° and 30° show that the pearlite steel curves were essentially the same at 30.5 mps (100 fps) velocity while the spheroidized steel curve was lower. For 61 mps (200 fps) the order of performance was the same but the amount of difference in erosion among the microstructures had changed.

A one-half hour duration test was conducted to determine if the pearlitic and spheroidized microstructures behaved the same after longer erosion times. The particle velocity used was 61 mps and the impact angle was 15°. The SiC particle size was slightly larger (280 μm diameter) than was used in the previous tests. The spheroidized structure once

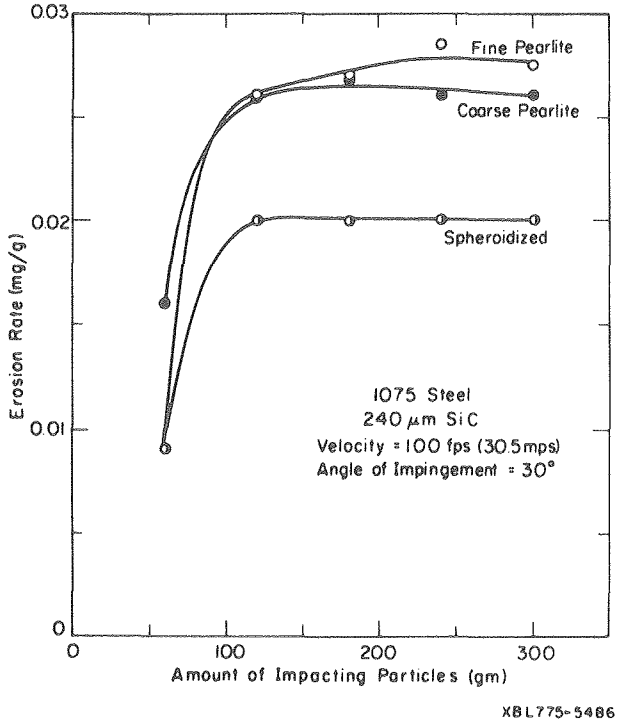

Fig. 3 - Plot of erosion rate versus amount of impacting particles (gm) for 1075 steel in three microstructures.

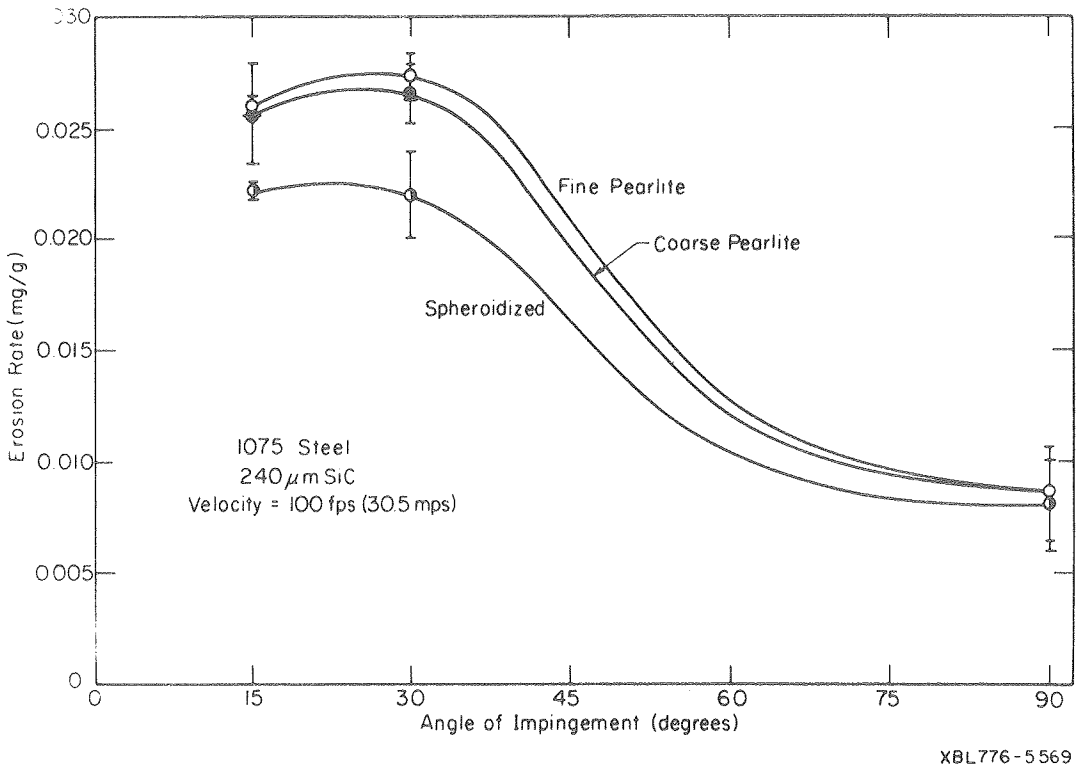

Fig. 4 - Plot of erosion rate vesus angle of impingement for 1075 steel in three microstructures.

again eroded less (wt. loss = 0.185 grams) than the pearlitic steel (wt. loss = 0.194 grams). The erosion resistance of the different microstructures is not what would have been expected from hardness data; the erosion increases with increasing hardness rather than decreasing. The fine pearlite material should have eroded the least since it was the hardest of the three microstructures. (R_B 100 compared to R_B 79 for the spheroidized steel).

Results of the single particle impact tests showed that the pearlitic and spheroidized structures exhibited markedly different mechanisms of erosion. The pearlitic steels typically showed fracturing of the cementite plates as the particle impacted the surface as seen in Figures 5 and 6. This type of surface fracture would be expected because of the brittleness of the cementite plates. The ferrite matrix, being very soft and ductile, appears to be torn away leaving the plates exposed. The spheroidized steel under single particle impact showed no severe cracking but rather exhibited a mechanism where the ferrite matrix was plastically deformed with carbide particles lying near or on the surface after impact (see Figure 7).

Cross sections of single particle impact craters resulting from large SiC particle impacts (1200 μm diameter) showed similar results to the SEM analysis of the surface of the single particle impact area. The pearlitic steel showed the cementite plates breaking off at the surface. It is also interesting to note that the brittle cementite plates below the surface are being bent in the process of crater formation, Figure 8. The cementite deformation without fracturing indicates a region of hydrostatic compression exists just beneath the surface.

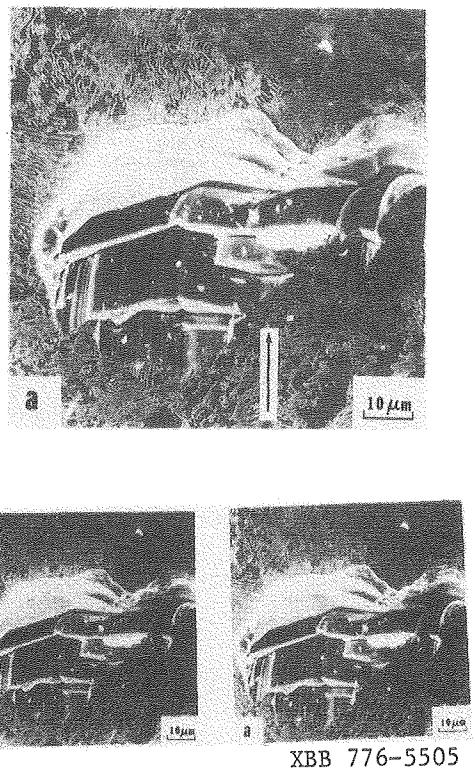

XBB 776-5505

Fig. 5 - Photomicrograph of single particle impact crater on 1075 steel (coarse pearlite using 240 μm SiC particles at V_p = 61 mps (200 fps), α = 15°. Stereo pair can be viewed with stereo viewer in back cover of ASM Handbook, Vol. 9.

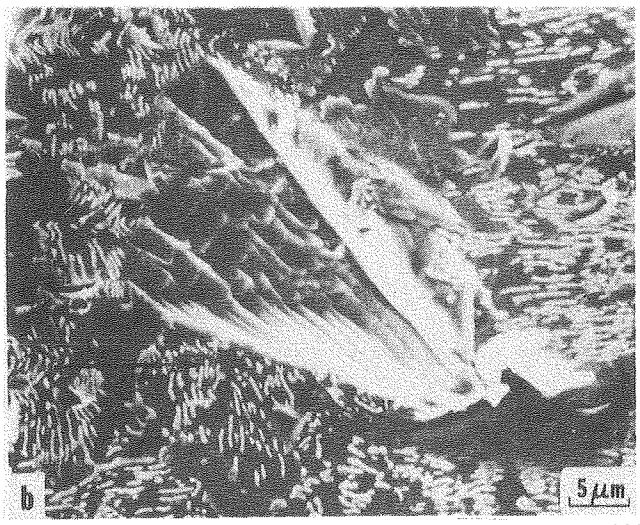

XBB 776-5635

Fig. 6 - Photomicrograph of a single particle impact crater on 1075 steel (coarse pearlite) using 240 μm SiC particles at a V_p = 107 mps (350 fps) and α = 15°.

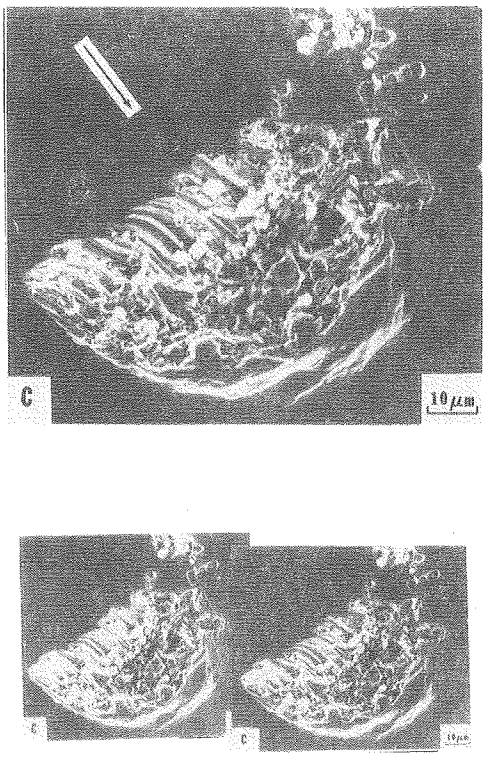

XBB 776-5506

Fig. 7 - Photomicrograph of a single particle impact crater on spherodized 1075 steel using 240 μm SiC at V_p = 71 mps (200 fps), $\alpha = 15^o$.

Multiple particle impact test samples in cross section showed microcracks forming below the surface. At particle velocities of 61 mps (200 fps) and 30.5 mps (100 fps) and angles of impingement of 15° and 30°, the spheroidized structure showed cracks at a depth of 20 μm, Figure 9. Under the same conditions the pearlitic steel showed cracks much nearer the surface (3 to 6 μm). At a 90° impact angle and a particle velocity of 61 mps, the spheroidized and pearlitic structures both showed that most of the subsurface cracking occurred in or very near the plastically deformed surface layer. Cracks were seen to a depth of ~15 μm below the surface.

The single particle impact study proved to be useful in explaining why the pearlitic structure eroded more than the spheroidized structure. Since the pearlitic steel showed fracturing on the eroded surface it is reasonable to assume the pearlitic steel's mechanism of material loss would be one in which the material could be driven from the surface in the form of chips that have cracked from the surface along brittle cementite lamellae (see Figure 5). The spheroidized steel showed no surface cracking and, therefore, would exhibit a mechanism in which much material would be plastically moved about with less material being actually driven from the surface (Figure 7).

The occurrence of subsurface void formation and cracking as shown in Figure 9 for the 1075 spheroidized steel is similar to the sub-surface fracture that has been observed in abrasive type wear by Suh and

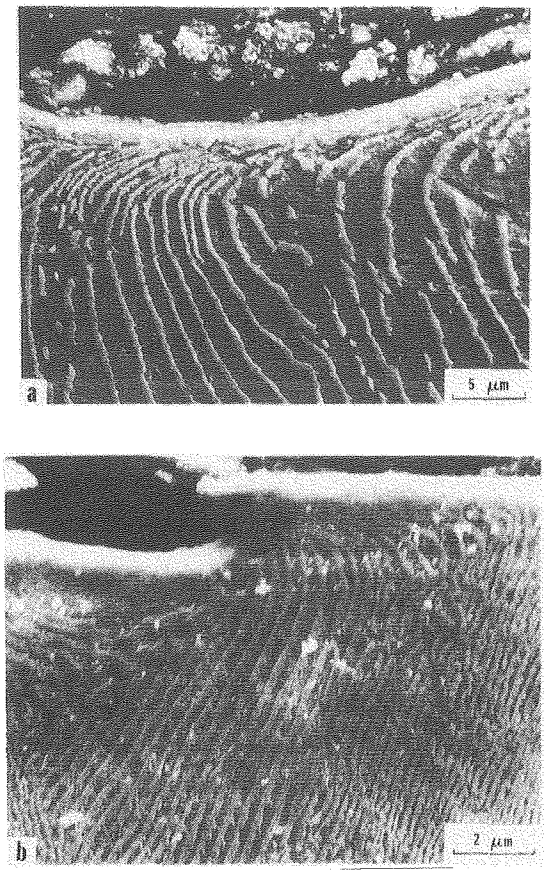

XBB 775-5258

Fig. 8 - SEM micrograph of cross section of 1075 steel (coarse pearlite) after multiple particle erosion with 240 μm SiC particles at V_p = 61 mps (200 fps), $\alpha = 30^o$.

Jahanmir (10). A model has been developed for the erosive wear observed in this investigation (11). It is based on the stress and strain distributions around second phase hard particles in a softer matrix material.

When the normal stress between the second phase particle and the matrix exceeds twice the shear yield strength of the material, a void can be generated beneath the surface that can subsequently propagate as sub-surface crack (12). The forces applied to the surface by impacting particles (Figure 10), cause plastic strains to occur in an area below the surface and hydrostatic compression to occur near the surface (see evidence in Figure 8). The sub-surface strains are associated with stress levels that distribute themselves in a region below the impacting particle.

Using the particle crater diameter from Figure 6 of approximately 30 μm as equal to 2a, the a distance from the surface inward in Figure 11 is approximately 15 μm. The region below the surface that exceeds the 2k stress level for void nucleation ranges from about 5 μm to 20 μm depending upon the impingement angle, α. This distance corresponds closely with the region of voids and cracking in Figure 9 for 1075 spheroidized steel eroded at an α of 30^o.

XBB 775-5263

Fig. 9 - SEM micrograph of cross section of 1075 steel (spherodized) after multiple particle erosion with 240 μm SiC at V_p = 61 mps (200 fps), $\alpha = 30^o$.

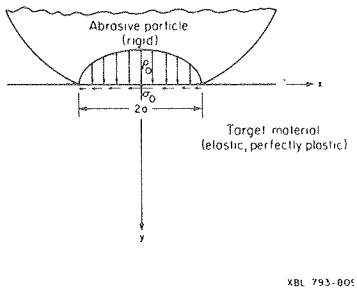

XBL 793-805

Fig. 10 - An idealized model of the contact between an impinging particle and the target surface.

Furthermore, if the total area in Figure 11 which exceeds the 2 k minimum stress level is plotted against the impingement angle, α, the curves of Figure 12 can be generated. The particles that cut rather than plough have a somewhat different, but similar stress distribution pattern to those that plough. Combining the non-cutting and cutting curves results in the dotted line curve shown. The general shape of this calculated curve, particularly its peak at an impingement angle of 15-20°, is approximately that observed in experimental erosion test curves for ductile metals. Also, the peak of the non-cutting or ploughing case near 30° matches that experimentally determined when spherical particles are used which do not cut.

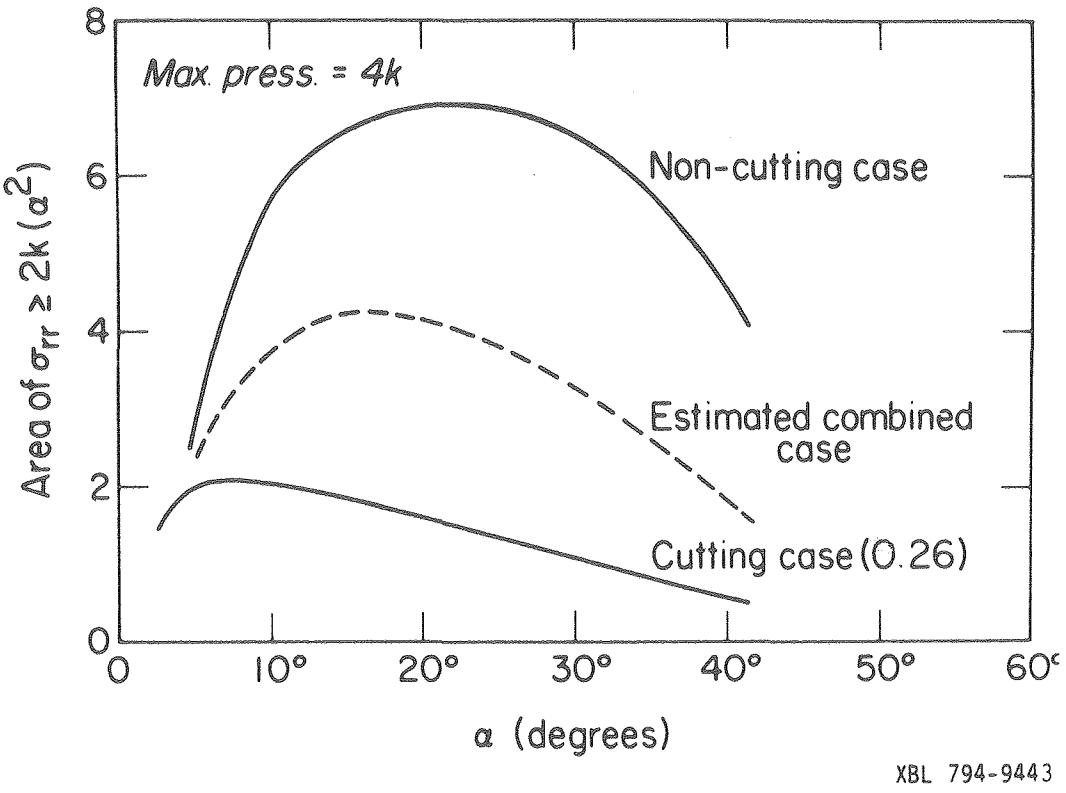

Fig. 12 - Area of interfacial normal stress around the second phase particle that exceeds the level for void initiation vs. impingement angle.

1075 steel was cold rolled to various percent reductions to cold work it and subsequently eroded with one 60 gm batch of 250 μm SiC particles. In as-spheroidized 1075 steel, the first batch of particles was not sufficient to achieve a constant level of cold work at the eroding surface (Figure 5).

Table 1 shows the effect of the various levels of cold working on the

Table I

Effect of Cold Work on Erosion of Spheroidized 1075 Steel

% Cold Worked	Hardness, VHN 1000 gm load	Initial Erosion Rate from 60gm SiC Particles
0	162	9.8×10^{-3} mg/g
20	242	10.3×10^{-3} mg/g
40	262	14.9×10^{-3} mg/g
60	288	16.6×10^{-3} mg/g
80	316	17.2×10^{-3} mg/g
	steady state erosion rate	22×10^{-3} mg/g

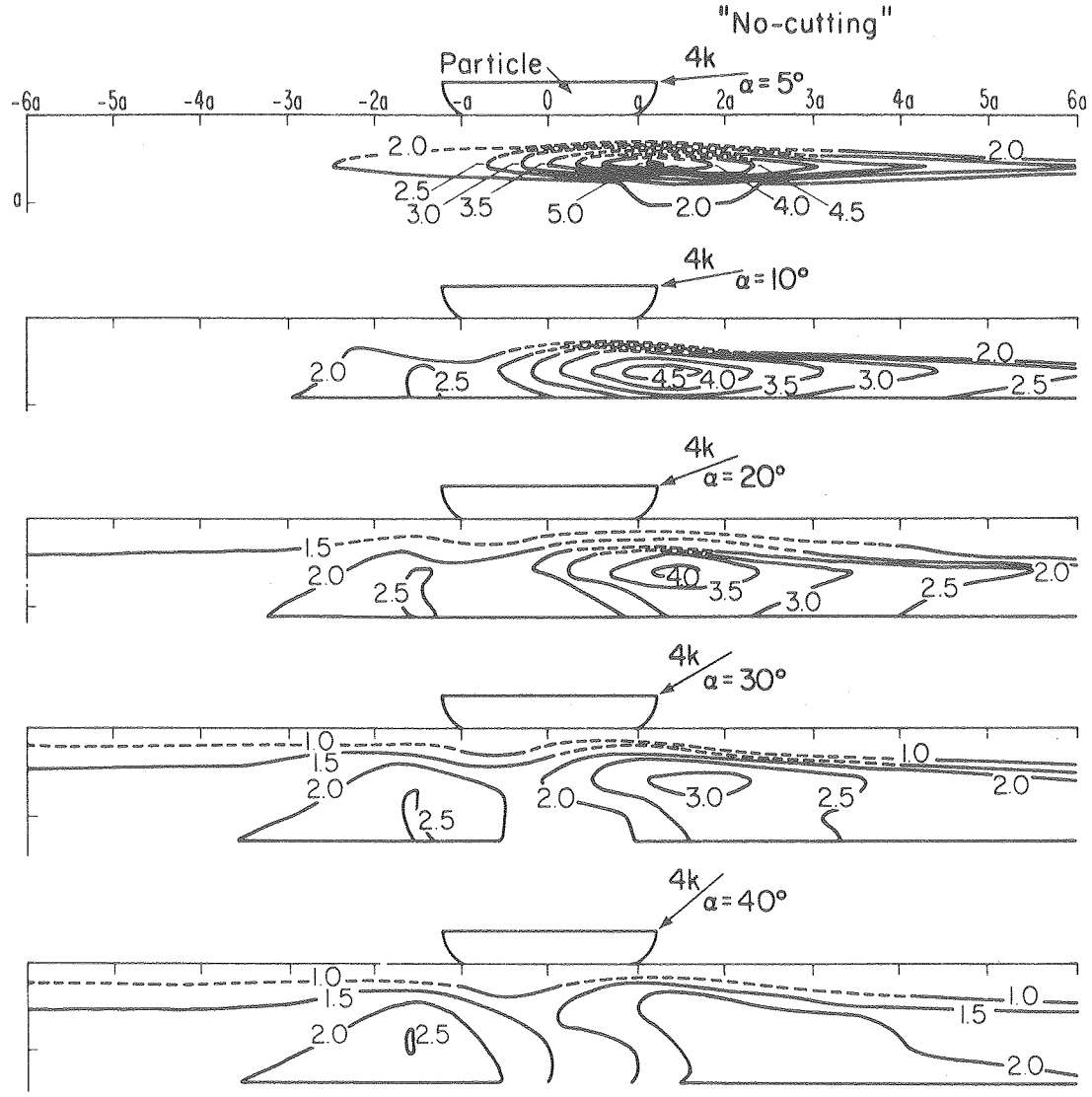

Fig. 11 - Contours of maximum normal stress at subsurface inclusions for impact pressure of 4K; "no cutting" case.

Thus, the plastic deformation which occurs beneath impacting particles induces stresses which can be calculated to cause the type of sub-surface void formation and fracture that is actually observed in two phase spheroidized steel when it is subjected to erosion.

Erosion as a Function of Work Hardnening

The impacting of erosive particles on the surface of a ductile metal results in high levels of strain that cause work hardening of the surface. Work hardening generally reduces the ductility of a material, in some materials to very low levels, while increasing its hardness. In order to investigate the effect of work hardening on erosion, spheroidized

erosion rate. It can be seen that as the material was cold worked, its erosion rate nearly doubled between the annealed condition and the 80% cold worked conditions. This is additional evidence that the ductility of the steel rather than its hardness can govern its rate of erosion.

Conclusions

1. Variations in the microstructure of a plain carbon steel, 1075, with little difference in hardness has a significant effect on the erosion behavior of the metal.

2. Ductility plays a major role in determining the erosion behavior of a material. The spherodized microstructure, which had the lowest hardness of the three microstructures of 1075 steel tested but the greatest ductility eroded the least. Also, as the metal was work hardened, reducing its ductility while increasing its hardness, the initial erosion rate increased.

3. An analytical model for erosion based on the calculation of the stresses and strains around 2nd phase hard particles in a softer matrix predict the occurrence and location of void generation and crack propagation beneath the surface and the shape of the erosion vs. particle impingement angle curve.

References

1. Finnie, I., "The Mechanisms of Erosion of Ductile Metals:, Proceedings of the 3rd U. S. National Congress on Applied Mechanics, 1958.

2. Finnie, I. and McFadden, D., "On the Velocity Dependence of the Erosion of Ductile Metals by Solid Particles at Low Angles of Incidence," Wear 48 1978, p. 81.

3. Bitter, J., "A Study of Erosion Phenomena, Parts 1, 2," Wear 6, 5 and 169, 1963.

4. Nielsen, J. and Gilchrist, A., "Erosion by a Stream of Solid Particles," Wear 11, 111, 1968.

5. Tilly, G., "A Two-Stage Mechanism of Ductile Erosion," Wear 23, 87, 1973.

6. Goodwin, J. E., Sage, W., and Tilly, G. P. "Study of Erosion by Solid Particles," Proceedings of the Institute of Mechanical Engineers, 184, 279-292, 1969.

7. L. Brass, "The Effects of the Microstructure of Ductile Alloys on Solid Particle Erosion," Masters Thesis, Dept. of Material Science and Engineering, University of California, Berkeley (1977).

8. D. Kleist, "One Dimensional-Two-Phase Particulate Flow," Masters Thesis, Dept. of Mechanical Engineering, University of California, Berkeley, (1977).

9. A. Ruff, L. Ives, "Measurement of Solid Particle Velocity in Erosive Wear," Wear, 35 (1975) 195.

10. Jahanmir, S. and Suh, N., "Mechanics of Sub-Surface Void Nucleation in Delamination Wear," Wear 44, pp. 17-38, 1977.

11. Jahanmir, S., "The Mechanics of Subsurface Damage in Solid Particle Erosion," submitted to Wear, April, 1979.

12. Argon, A. S. and Im, J., "Separation of Second Phase Particles in Spheroidized 1045 Steel, Cu-0.6 Pct Cr Alloy, and Maraging Steel in Plastic Straining," Met Trans 6A, pp. 839-851, 1975.